

PCCP

Accepted Manuscript



This is an *Accepted Manuscript*, which has been through the Royal Society of Chemistry peer review process and has been accepted for publication.

Accepted Manuscripts are published online shortly after acceptance, before technical editing, formatting and proof reading. Using this free service, authors can make their results available to the community, in citable form, before we publish the edited article. We will replace this *Accepted Manuscript* with the edited and formatted *Advance Article* as soon as it is available.

You can find more information about *Accepted Manuscripts* in the [Information for Authors](#).

Please note that technical editing may introduce minor changes to the text and/or graphics, which may alter content. The journal's standard [Terms & Conditions](#) and the [Ethical guidelines](#) still apply. In no event shall the Royal Society of Chemistry be held responsible for any errors or omissions in this *Accepted Manuscript* or any consequences arising from the use of any information it contains.

Understanding the ionic liquid $[\text{NC}_{4111}][\text{NTf}_2]$ from individual building blocks: An IR-spectroscopic study

Kenny Hanke¹, Matin Kaufmann, Gerhard Schwaab, and Martina Havenith*

Department of Physical Chemistry II, Ruhr-University Bochum, D-44801 Bochum

Conrad T. Wolke¹, Olga Gorlova and Mark A. Johnson*

Department of Chemistry, Yale University, New Haven, CT 06520, USA

Bishnu Kar and Wolfram Sander

Department of Organic Chemistry II, Ruhr-University Bochum, D-44801 Bochum

Elsa Sánchez-García

Department of Theory, Max-Planck-Institut für Kohlenforschung, Kaiser-Wilhelm-Platz 1, D-45470 Mülheim an der Ruhr

Abstract:

This study explores at the molecular level the interactions underlying the IR spectra of the ionic liquid $[\text{NC}_{4111}][\text{NTf}_2]$ and its deuterated isotopomer $[\text{d}_9\text{-NC}_{4111}][\text{NTf}_2]$ by first isolating the spectra of charged ionic building blocks using mass-selective CIVP spectroscopy and then following the evolution of these bands upon sequential assembly of the ionic constituents. The spectra of the (1,1) and (2,2) neutral ion pairs are recorded using superfluid helium droplets as well as a solid neon matrix, while those of the larger charged aggregates are again obtained with CIVP. In general, the cluster spectra are similar to that of the bulk, with the (2,2) system displaying the closest resemblance. Analysis of the polarization-dependent band intensities of the neutral ion pairs in liquid droplets as a function of external electric field yields dipole moments of the neutral aggregates. This information allows a coarse assessment of the packing structure of the neutral pairs to be antiparallel at 0.37 K, in contrast to the parallel arrangement found for the assembly of small, high-dipole neutral molecules with large rotational constants (e.g., HCN).

The role of an extra anion or cation attached to both the (1,1) and the (2,2) ion pairs to form the charged clusters is discussed in the context of an additional remote, more unfavorable binding site intrinsic to the nature of the ionic IL clusters and as such not anticipated in the bulk phase. Whereas for the anion itself only the lowest energy *trans* conformer was observed, the higher clusters showed an additional population of the *cis* conformer. The interactions are found to be consistent with a minimal role of hydrogen bonding.

Keywords: IR Spectroscopy, Ionic Liquids, Helium Nanodroplets, CIVP Spectroscopy

***Corresponding Authors:** martina.havenith@rub.de and mark.johnson@yale.edu

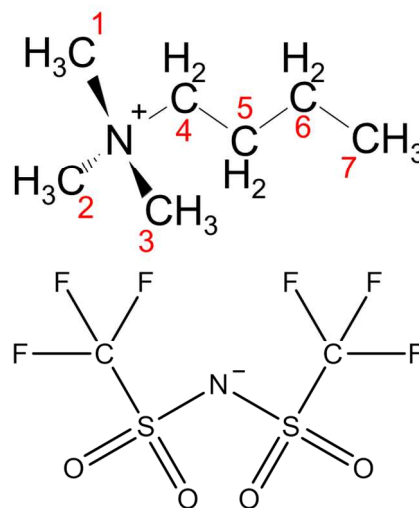
⊥ both authors contributed equally

I. Introduction

In recent years, room temperature ionic liquids (IL) have generated considerable interest in both basic science and industrial applications. These can be considered organic salts, and exhibit remarkable properties that make them an ideal platform for the generation of tailored materials. For example, because ILs have both low melting points (< 373 K) and very low vapor pressures, they are considered environmentally friendly.¹ And because their bulk properties (e.g. liquid range, heat capacity, viscosity, etc.) are highly dependent on the detailed molecular structures of the ionic constituents, different combinations of cations and anions provide a common platform for a large variety of controlled solvents.²⁻⁴ Applications for ILs include organic and inorganic synthesis, catalysis⁵⁻⁹ (including bio-catalysis),¹⁰⁻¹² electrochemistry and CO₂ processing.¹³⁻¹⁵ In the energy sector they play a role in batteries,¹⁶⁻¹⁸ fuel cells,¹⁹⁻²² and even rocket fuels.²³ Despite the fact that almost a decade has passed since their first successful distillation by Earle et al.²⁴ in 2006, the local molecular interactions that underlie the macroscopic properties of the bulk material remain a challenge and are presently under vigorous investigation.²⁵⁻²⁸ For example, although Coulomb forces are clearly the strongest interactions among the ionic constituents of an IL, hydrogen bonding and dispersion forces have also been invoked to rationalize the local structural motifs.²⁹⁻³¹

Here we are concerned with the intramolecular distortions and docking arrangements at play in the *n*-butyltrimethylammonium bis(trifluoromethylsulfonyl)imide [NC₄₁₁₁][NTf₂] system, with molecular structures of the ionic constituents displayed in the Scheme.

Fig. 1 presents the bulk FT-IR absorption spectrum of liquid [NC₄₁₁₁][NTf₂] at room temperature. The observed bands appear in well-separated, localized regions of the spectrum, with those arising from the (NTf₂)⁻ anion colored blue while those from the (NC₄₁₁₁)⁺ cation colored red, with the various groups primarily responsible for transitions indicated at the top.



Scheme. Structure of the cation (top) and anion (bottom) ionic constituents of the room temperature ionic liquid [NC₄₁₁₁][NTf₂]. The numbering scheme for the carbon atoms in the cation is shown in red.

The Raman spectrum of partially crystallized $[\text{NC}_{4111}][\text{NTf}_2]$ has also been reported and analyzed in the frequency range up to 1100 cm^{-1} by Ribeiro et al.,³² who noted that different crystalline structures could be prepared by changing the cooling rate. The spectral differences could then be explained by the spectral signatures associated with the specific anion-cation docking arrangements kinetically trapped in the heterogeneous mixtures. In our approach, we isolate cold, composition-selected $(\text{NC}_{4111})^+_n (\text{NTf}_2)^-_m$ clusters and analyze their vibrational spectra in order to reveal how the features in the spectrum of the bulk liquid evolve from the intrinsic behavior of the ions, first through local perturbations caused by the close packing of the ionic constituents in small clusters. We focus on the $[\text{NC}_{4111}][\text{NTf}_2]$ system as an archetypal IL for which hydrogen bonding plays a minimal role due to the low acidity of the alkyl CH groups on the $(\text{NC}_{4111})^+$ cation.³³ The selection of $(\text{NTf}_2)^-$ as the counterion was driven by the fact that this species is the anion of choice in contemporary IL research.^{34,35} We first report the vibrational spectra of the individual ionic components, information that allows us to follow the evolution of the spectra as the components are assembled incrementally into neutral ion pairs and then charged clusters with an odd number of ionic constituents. This study thus adds to the rapidly increasing body of work characterizing the interactions at play in ILs using cold cluster methods, with previous reports being primarily concerned with quantifying the extent of H-bonding in imidazolium-based (e.g., EMIM) systems.³⁶⁻³⁹ A recent comparison of IR and UV_VIS bulk spectra of 1-Ethyl-3-methylimidazolium bis(trifluoromethylsulfonyl)imide with DFT and MP calculations for the gas phase and in a continuum solvent yielded an –surprisingly– an improved agreement of the gas phase predictions with the experimental bulk spectra.^{40,41}

The authors concluded that for a description of bulk spectra in ionic liquids the influence of the surrounding ion pairs cannot be adequately described as an effective dielectric medium. In the present work we have therefore decided to perform an experimental bottom-up approach to unravel the nature of intermolecular binding in case of ionic liquids.

Spectra of the charged species were obtained by mass-selective cryogenic ion vibrational predissociation CIVP spectroscopy,^{42,43} while those of the neutral ion pairs were obtained with helium nanodroplet⁴⁴⁻⁴⁷ and solid matrix isolation methods.⁴⁸ CIVP uses weakly bound messenger tags to perform composition-selected, infrared action spectroscopy on charged building blocks of the type $(\text{NC}_{4111})^+_n (\text{NTf}_2)^-_m$, with $n = m \pm 1$. Helium nanodroplet

spectroscopy accesses the infrared spectra of neutral ion pairs and clusters of two or more ion pairs in a superfluid helium matrix.^{37,49} Neon matrix isolation spectroscopy was also used to characterize the neutral clusters, where the species are embedded in a solid layer of condensed neon cooled to cryogenic temperatures. Thus, by combining the complementary spectroscopic capabilities of several different laboratories, we obtain a complete, “bottom up” picture of how the individual ions and local perturbations contribute to the spectrum of the bulk material.

II. Experimental Details

N-butyltrimethylammonium bis(trifluoromethylsulfonyl)imide [NC₄₁₁₁][NTf₂] was purchased from Sigma-Aldrich. Nonadeuteriobutyltrimethylammonium bis(trifluoromethylsulfonyl)imide [d₉-NC₄₁₁₁][NTf₂] was synthesized by ChiroBlock GmbH.

IR-spectra were recorded in the Bochum helium cluster machine which is described in detail elsewhere.⁵⁰ Helium nanodroplets are formed by expanding precooled Helium (12.7 K) under high pressure (50 bar) through a 5 μm nozzle into vacuum, cooling down to 0.37 K by evaporative cooling and shaped into a molecular beam by a skimmer. In a second chamber [NC₄₁₁₁][NTf₂] is evaporated in a cylindrical stainless steel oven with an inner hole diameter of 5 mm which can be heated with a heating band up to 600 K. Sample temperature and oven surface temperature are monitored by a PT100 temperature sensor placed near the reservoir and a type K thermocouple between the steel cylinder and the heating band. Test measurements yielded an oven

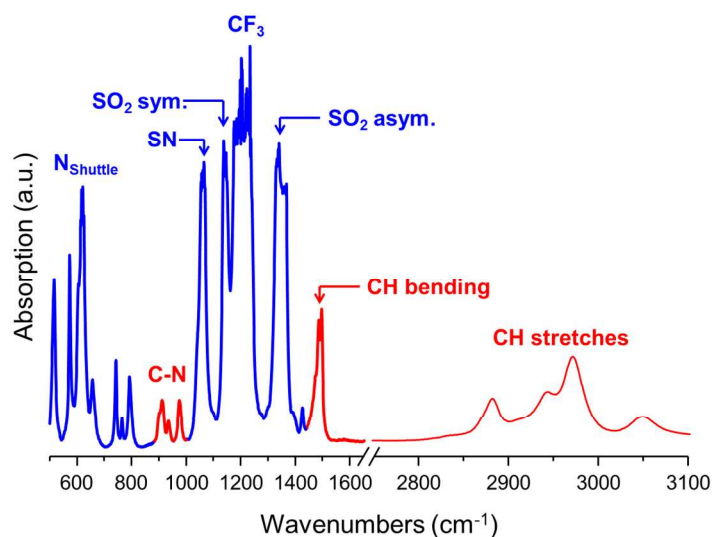


Figure 1. Bulk FT-IR spectrum of 300K [NC₄₁₁₁][NTf₂]. Parts of the spectrum which are attributed to anion and cation IR bands are marked in blue and red, respectively, along with crude assignments to functional groups indicated at the top.

temperature of 450(1) K as optimal temperature for the pick-up of single ion pairs of $(\text{NC}_{4111})^+(\text{NTf}_2)^-$, since no mass signals of fragments of larger clusters could be observed at this temperature.

The seeded beam is further guided through the multipass chamber which consists of two parallel gold mirrors used to intersect the clusters by a tunable Aculight Argos continuous wave Optical Parametric Oscillator (OPO) laser system. By simultaneously ionizing the droplets by electron impact the ion intensities are monitored through a Pfeiffer QMS4224 quadrupole mass spectrometer. When the frequency of the OPO is tuned to a vibrational transition of the IL, the absorbed energy is transferred to the helium droplet which loses the excess energy by evaporation of He atoms. Shrinking of the nanodroplets directly translates into the reduction of the ionization cross section, leading to depletion of ion signal. To monitor the reduction of signal intensity the QMS can either be used as a high pass filter with the lowest mass set to $m/z = 8$ amu/e or set to a specific mass-to-charge ratio. Tracking of the ion signal as a function of photon energy from 2800 to 3100 cm^{-1} results in the IR spectra of the ion pair in that frequency range. The laser beam is amplitude modulated by a chopper at a frequency of about 20 Hz for phase sensitive detection and the signal is demodulated by a lock-in amplifier connected to the QMS. For the measurement of the permanent dipole moment and the vibrational transition moment angle (VTMA)⁵¹ the multipass cell is equipped with two electrodes orthogonal to the mirrors and spaced 6.3 mm apart where a voltage of up to ± 20 kV can be applied.

Cryogenic ion vibrational predissociation (CIVP) IR-spectra were recorded using the cryogenic ion spectrometer at Yale University. This machine is described in detail elsewhere and only a short summary of the technique will be given here. A 2 mM solution of $[\text{NC}_{4111}] [\text{NTf}_2]$ in acetonitrile was ionized via electrospray ionization. The resulting $(\text{NC}_{4111})^+_n(\text{NTf}_2)^-_m$ clusters were then guided by RF only quadrupoles and electrostatic ion optics into a Paul trap where they were stored for 90 ms, cooled down to 25 K and tagged with N_2 by pulsing a buffer gas into the trap. The tags were ejected into a TOF mass spectrometer. When the OPO/OPA laser system is scanned over an infrared transition of the ion, the excess energy is redistributed via IVR eventually leading to the loss of the lightly bound messenger tag. IR-spectra in the range of 600 to 3400 cm^{-1} are recorded by monitoring the evaporation of N_2 as a function of laser frequency.

Matrix isolation experiments were performed using a Sumitomo compressor and cold head, which can be cooled down to 4 K. The IL was heated in an oven up to 480 K. Single ion pairs were deposited with large excess of Ne (Neon 5.0, Air Liquide) on a cold CsI window attached to the cold head, by heating a sample of [NC₄₁₁₁] [NTf₂] in a sublimation oven consisting of a quartz tube with a diameter of 7.5 mm and a length of 50 mm, heated electrically with a tantalum wire wrapped around the tube. The drop of ionic liquid was kept in a smaller quartz tube inside the oven. A Bruker IFS66 FT-IR spectrometer was used to record the infrared spectra in the frequency range between 400 and 4000 cm⁻¹ with a resolution of 0.5 cm⁻¹. FT-IR spectra of the bulk liquid were recorded with a commercial PerkinElmer Spectrum 100 FT-IR spectrometer at a resolution of 4 cm⁻¹. The measurement cell had a thickness of 50 μm and was equipped with diamond windows.

III. Computational Methods

Ab initio calculations were carried out using the Turbomole package.⁵² Minimum energy structures were obtained by geometry optimization of 300 random structures of the bare anion and cation using the B3LYP functional^{53,54} with the aug-cc-pVDZ basis set.^{55,56} In the same way, 1000 random structures of the neutral ion pair were optimized at the B3LYP/SVP⁵⁷ level of theory. For all DFT calculations, the dispersion correction⁵⁸ was used as implemented in the Turbomole package⁵⁹. The calculated structures were reoptimized at the MP2 level of theory⁶⁰ as implemented in the Turbomole package⁵⁹ and the harmonic frequencies were calculated⁶¹⁻⁶³. We chose the cc-pwCVTZ basis set⁶⁴ for the isolated anion and the cc-pVTZ basis set for the isolated cation^{65,66}. Calculations on the ion pair were carried out with the aug-cc-pwCVDZ basis set⁶⁴. As typical when comparing calculated and experimental spectra, the predicted frequencies were scaled according to different spectral regions (bare anion: 0.968; bare cation (2000-3100 cm⁻¹): 0.940; bare cation (600-1500 cm⁻¹): 0.979; ion pair (2800-3100 cm⁻¹): 0.945). These factors were chosen in order to match key IR transitions, where a definite assignment was possible. The predictions for the permanent dipole moment and the vibrational transition moment angle (VTMA) of the neutral ion pair were also obtained by the MP2 calculations.

Quantum mechanics molecular dynamics simulations (QM MD) were carried out at 500 K with the ChemShell code^{67,68} using Turbomole for the QM region which was formed by the

ion pair and treated at the B3LYP/SVP level of theory, using dispersion correction. The time step was 1 fs, and the total length of the simulation 15 ps. A temperature of 500 K was chosen which corresponds to the evaporation temperature of the IL before pick up. Choosing for a higher temperature allowed to sample the entire conformational space of the ion pair.

IV. Results and Discussion

IVA. Characterization of the isolated ionic components

IVA.1 The NC_{4111}^+ cation

Figure 2 presents the lowest energy isomers recovered for the bare $(\text{NC}_{4111})^+$ cation at the MP2/cc-pVTZ level of theory. The conformation of the cation's butyl group is labeled following the Klyne-Prelog nomenclature,⁶⁹ e.g. the linear conformer where all dihedral angles are 180° is labeled anti-periplanar/anti-periplanar (ap/ap) with respect to the $\text{N}-\text{C}^4-\text{C}^5-\text{C}^6$ and $\text{C}^4-\text{C}^5-\text{C}^6-\text{C}^7$ dihedral angles. After the zero point vibrational energy correction, the antiperiplanar/antiperiplanar (ap/ap) arrangement was determined to be the minimum energy isomer. This conformation of the butyl moiety is also called *trans/trans* or anti/anti in other publications and is found to be the minimum energy structure in the 1-butyl-3-methylimidazolium tetrafluoroborate [BMIM][BF₄] and N-butyl-N-methylpyrrolidinium bis(trifluoromethylsulfonyl)imide [P₁₄][NTf₂] ionic liquids.^{70,71} Higher energy

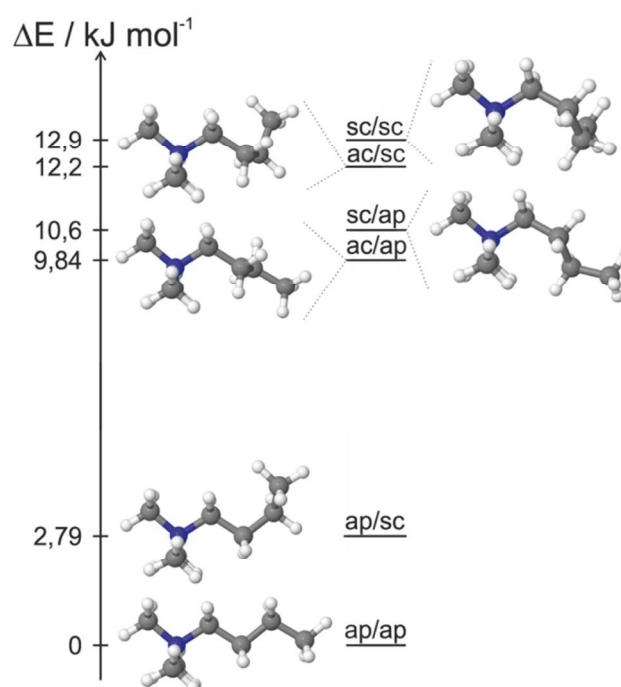


Figure 2. Local minimum conformers of the bare cation obtained with MP2/cc-pVTZ. The structures are labeled according to their $\text{N}-\text{C}^4-\text{C}^5-\text{C}^6$ and $\text{C}^4-\text{C}^5-\text{C}^6-\text{C}^7$ dihedral angles, as indicated in the Scheme, with each ZPVE corrected electronic energy shown on the right hand axis.

structures for $(\text{NC}_{4111})^+$ denoted ap/sc, ac/ap, sc/ap, ac/sc and sc/sc configurations are calculated at +2.79, +9.84, +10.6, +12.2 and +12.9 $\text{kJ}\cdot\text{mol}^{-1}$, respectively. While the difference in energy of the ap/sc conformer compared to the ap/ap groundstate is still in the order of thermal energy ($kT = 3.74 \text{ kJ}\cdot\text{mol}^{-1}$) even at the elevated evaporation temperature of 450 K all other conformers should be much less populated.

The experimental CIVP spectra (black) of two $(\text{NC}_{411})^+$ isotopomers (all H and all D substitution of the butyl group) are displayed in the middle of Fig. 3, along with the harmonic predictions red, top and bottom) for the (ap/ap) structure indicated in Fig. 2. Several key vibrational motifs are color-coded with block rectangles according to their assignments to particular groups. The methyl CH bending motions between 1400 and 1500 cm^{-1} (green) are predicted to be dominated by the asymmetric in-phase and out-of-phase (δ_a) collective motions of all three CH_3 groups at 1486 cm^{-1} and 1468 cm^{-1} , where the latter is overlapped by the in-phase bending of only two methyl groups. A third band at 1409 cm^{-1} is assigned to the symmetric out-of-phase bending of all three methyl groups. The only other bands

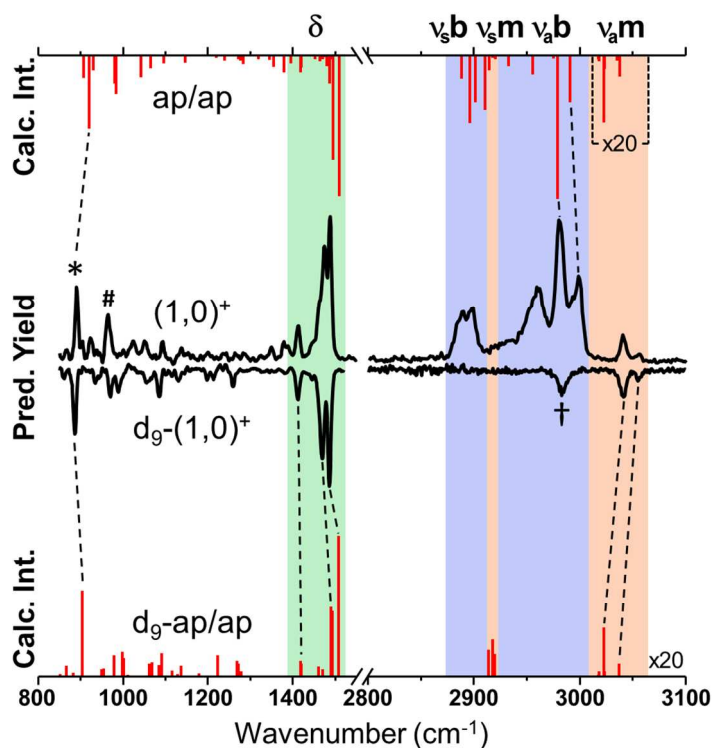


Figure 3. From top to bottom: harmonic spectrum (red) of the ap/ap $(\text{NC}_{4111})^+$ conformer obtained at the MP2/cc-pVTZ level (scaled by 0.979 between 600-1500 cm^{-1} and 0.94 between 2000-3100 cm^{-1}); CIVP spectra of the undeuterated (1,0) and deuterated d_9 -(1,0) cation; predicted spectrum (red) of the ap/ap conformer of the deuterated cation obtained at the same level and scaling. Features are color-coded for each type of vibration: methyl CH stretches, ν_{sm} and ν_{am} in orange, butyl stretches, ν_{sb} and ν_{ab} , in blue, and methyl CH bends, δ , in green. Note that the vertical axes are arbitrarily scaled on either side of the break in the abscissa.

in the fingerprint region of the spectrum carrying sufficient intensity for an assignment include the amide-butyl stretch at 893 cm^{-1} (*) and the near degenerate in and out-of-plane nitrogen shuttle between two methyl groups at 963 cm^{-1} (#).

The contributions to the 2800 to 3100 cm^{-1} range of the vibrational spectra originate from either the methyl groups (m, orange) or the butyl chain (b, blue) and are further divided into asymmetric and symmetric stretching collective modes, ν_s and ν_a . A complete list with all band assignments of this spectral region is provided in Table 3 of the SI. The large intensity of IR features containing the butyl CH stretches complicates unambiguous identification of CH stretches associated with the methyl groups. Therefore, selective deuteration was used in which all nine hydrogens of the butyl group were replaced by deuterium atoms, thus removing all butyl contributions from this spectral region while leaving the methyl bands intact. The IR spectrum of the heavier d_9 -(1,0) cation is plotted against that of the undeuterated species as the inverted black trace in Fig. 3, along with the red stick harmonic prediction, displayed in the bottom trace. As a spectral verification of the successful deuteration, we observed a slight red-shift of the amide-butyl stretch (*, Fig. 3) due to the increased reduced mass, while the in-plane nitrogen shuttle (#) undergoes a blue-shift as the heavier butyl forms a more rigid base for this motion. Both shifts clearly demonstrate the fact that only the hydrogens of the butyl chain are substituted for heavier deuterium isotopes. The CD stretches of the d_9 -butyl group strongly red-shift, completely exposing the decongested pattern of methyl CH stretches and thus allowing a better understanding of the underlying molecular physics taking place in the methyl groups.

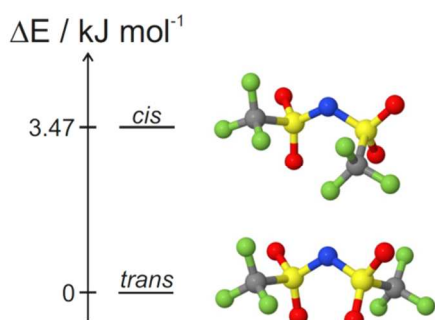


Figure 4. The local minimum conformers of the bare anion obtained with MP2/cc-pwCVTZ with each ZPVE corrected electronic energy shown on the right hand axis. The *cis* and *trans* notation refers to the C-S-S-C dihedral angle.

Bands in the spectrum of the deuterated d_9 -(1,0) cation at 3041 cm^{-1} and 3055 cm^{-1} can be assigned with confidence to the in-phase, $\nu_a^{i,p}$ and an out-of-phase asymmetric stretch vibration $\nu_a^{o,p}$ of the methyl groups attached to the central nitrogen, respectively. Surprisingly, however, the experimentally observed band at 2983 cm^{-1} (marked by †), is not reproduced by the electronic structure calculations. Theory predicts the symmetric methyl stretching fundamental

ν_3 at 2920 cm^{-1} , in a region where no IR activity is present in the experimental spectrum. One explanation for this deviation is that strong quartic coupling gives rise to the 65 cm^{-1} blue shift (i.e., negative anharmonicity), while it is also possible that the observed 2983 cm^{-1} band is actually due to overtone and combination bands involving CH bends, with their corresponding fundamental located at 1486 cm^{-1} . Such a situation was pervasive, for example, in a previous report of the bands in the imidazolium based ionic liquids (e.g., EMIM).³⁷ Without further anharmonic analysis beyond the scope of this paper, this assignment must be considered an open question at this time, and thus not particularly useful in our structural characterization of the IL interactions which is our primary focus.

Returning to the all-H cation, the bands between 2800 and 3100 cm^{-1} , which are not present in the spectrum of the heavier isotopologue, necessarily originate from motions containing the n-butyl group. Hence, based on the harmonic predictions, the doublet at 2999 cm^{-1} and 2981 cm^{-1} and the broad features around 2959 cm^{-1} are assignable to the in-phase and out-of-phase vibrations involving the entire butyl chain and the asymmetric CH stretches of the terminal CH_3 group, respectively. The calculations indicate that the doublet centered at around 2893 cm^{-1} likely results from the symmetric butyl vibrations, where the feature higher in energy involves the CH_2 group next to the amide center.

IVA.2 The NTf_2^- anion

Ab initio calculations of the anion $(\text{NTf}_2)^-$ at the MP2/cc-pwCVTZ level of theory yielded two stable conformers with C-S-S-C dihedral angles of 175° and 41° , labeled ‘trans’ and ‘cis’ in Fig. 4, respectively. The *trans* conformer is predicted to be more stable, with the minimum *cis* isomer predicted to lie 3.47 kJ mol^{-1} higher in energy (after ZPVE correction). This result is in agreement with previous theoretical results by Brouillette et al. and Herstedt et al.^{72,73}

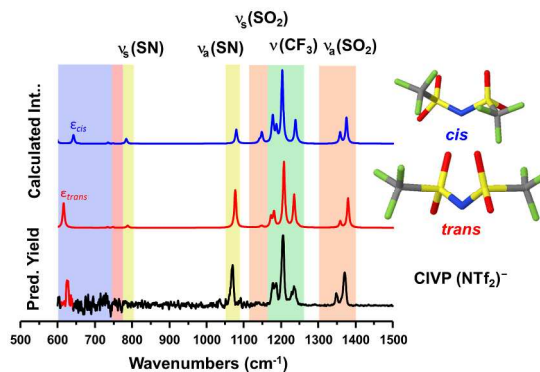


Figure 5. Comparison of the calculated harmonic spectra of the two minimum energy conformers, *cis* and *trans*, to the experimental C1VP spectrum of $(\text{NTf}_2)^-$. Block color bars correspond to a displacement of normal modes labeled at the top. Key bands near 600 cm^{-1} of particular importance in the determination of the conformer composition are denoted ϵ_{cis} , ϵ_{trans} , respectively.

Fig. 5 presents the predicted vibrational spectra of the *cis* and the *trans* anion conformers along with the experimental CIVP spectrum of the bare anion. Vibrations in the calculated spectra are labeled according to the largest contributions of specific bond motifs in the normal mode analysis.

The harmonic transitions of the *trans* and *cis* conformers show a very similar pattern except for the low frequency range between 600 and 670 cm^{-1} and a pronounced feature labeled α at 1133 cm^{-1} . For the *trans* conformer an intense band is predicted at 616 cm^{-1} , assigned to a combined motion involving the CSN bending deformation $\delta(\text{CSN})$ and the out-of-phase umbrella motions of the CF_3 and SO_2N groups, nearly isoenergetic with a second weaker feature at 615 cm^{-1} involving $\delta(\text{SNS})$ and $\delta(\text{NSO})$ bending. For the *cis* conformer, these two bands split significantly, where the latter $\delta(\text{SNS})$ bend blue shifts to 642 cm^{-1} gaining intensity, while the $\delta(\text{CSN})$ deformation loses intensity and red-shifts to 595 cm^{-1} . The α band is due to the symmetric SO_2 stretch ($\nu_s(\text{SO}_2)$) and is much stronger in the *cis* spectrum. In the experimental CIVP spectrum, a single intense peak at 626 cm^{-1} is observed at low energy and there is no significant activity near the telltale α band, together leading to the conclusion that the uncomplexed bare anion predominately exists in the *trans* configuration.

IVB. Comparison of bare ion spectra with that of the room temperature IL

Before engaging the behavior of the assembled ions, it is useful to first establish to what extent the spectra of independent ions are preserved in that of the bulk material. Figure 6 compares the spectra of the NC_{411}^+ (blue) and $(\text{NTf}_2)^-$ anions (red) with the FTIR spectrum of the bulk IL at room temperature (black). It is clear that many of the bulk bands are, indeed already present in the independent ions, and as such are not useful in the analysis of the intermolecular interactions beyond their qualitative implication that the ions are essentially intact even when

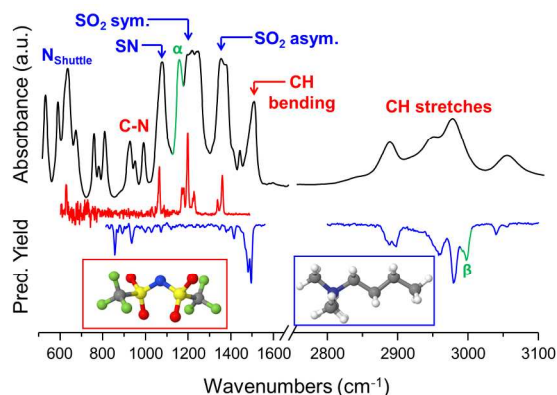


Figure 6. Comparison of the individual ionic liquid constituents $(\text{NC}_{411})^+$ (blue) and $(\text{NTf}_2)^-$ (red) to the bulk FT-IR, (top black). The peak labelled α is anticipated for the *cis* $(\text{NTf}_2)^-$ conformer, while the β feature arises from the butyl group in bare $(\text{NC}_{411})^+$ ion and is not evident in the bulk spectrum.

closely packed in the condensed phase. Two transitions labeled α and β in Fig. 6, are significantly different in the bare ion spectra compared to that of the higher clusters and thus are clear reporters of the interactions at play. One of these, the β band in the cation near 3000 cm^{-1} , is missing in the bulk spectrum and was already assigned to the asymmetric CH stretching motions on the butyl group through the selective H/D isotopic substitution study (ν_{ab} in top of Fig. 3).

This suggests that these transitions are red shifted into the main envelope of the bulk absorption, which in turn indicates that this group is strongly interacting with the anion. The α transition, on the other hand, is not present in the spectra of either of the independent ions, but is interestingly close to the calculated band for the higher energy *cis* isomer of the anion, thus raising the interesting scenarios where the conformers are either trapped in metastable states in the condensed phase or are stabilized by complexation with a counter ion. With these observations in mind, we next turn to the assembly of the ions, first into ion pairs and then the tertiary ionic clusters.

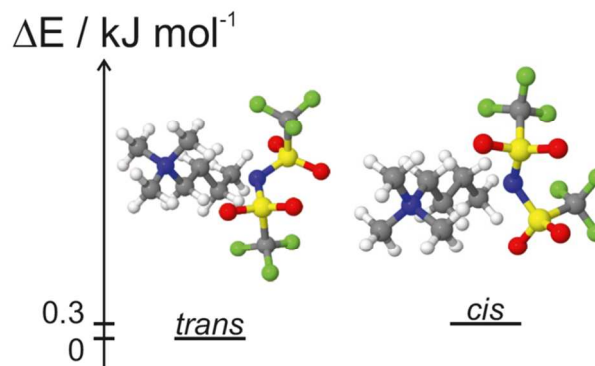


Figure 7. $[\text{NC}_{4111}][\text{NTf}_2]$ with the anion in transoid (left) and cisoid (right) and cation in ap/ap conformation. The energies shown are the relative ZPVE corrected electronic energies.

IVC. The neutral ion pairs

Observation of the detailed evolution of the isolated ion IR bands with the incremental addition of the ionic constituents provides an excellent opportunity to understand the fundamental molecular physics of the electrostatic interactions driving the microscopic assembly. To set the stage, we first consider the structure of the (1,1) ion pair. Identification of likely binding motifs was accomplished using the QM MD simulation at the B3LYP-D/SVP level of theory at a temperature of 500 K, for which a 15 ps animation of calculated frames with 1 fs time intervals can be found in the SI. Here, the cation mostly adopts the ap/ap conformation, but all isomers depicted in the SI were observed, indicating a potential energy surface with many local minima. Fig. 7 shows the optimized structures for the ion pair with the anion in *trans* and

cis orientation. Note that while the cation remains in its energetically favored ap/ap configuration, the energies of the two isomers are now much closer in energy (3.47 vs. 0.3 kJ/mol), suggesting that the higher energy *cis* isomer can play a larger role in the equilibrium ensembles even at low temperature. The vibrational modes of the unscaled predictions for both geometries are listed in Tab. 1 in the SI for the bands associated with motions of the anion.

Figure 8 highlights two regions of the IR spectra displayed by the ion pair in helium droplets (denoted Helium (1,1)) and in the neon matrix (denoted Neon(1,1)), and compares these patterns with those observed for the ionic (1,0), (2,1) and (3,2) clusters and finally to the room temperature FT-IR bulk spectrum (FTIR (bulk)). Note that ion pairs corresponding to the (1,1) and (2,2) compositions were obtained using the helium droplet approach and will be formed following rapid cooling. In particular, by monitoring the abundance of $m/z = 512$, which corresponds to the mass of an ion pair plus a cation in a helium droplet, the spectrum of a neutral complex comprising *at least* two ion pairs

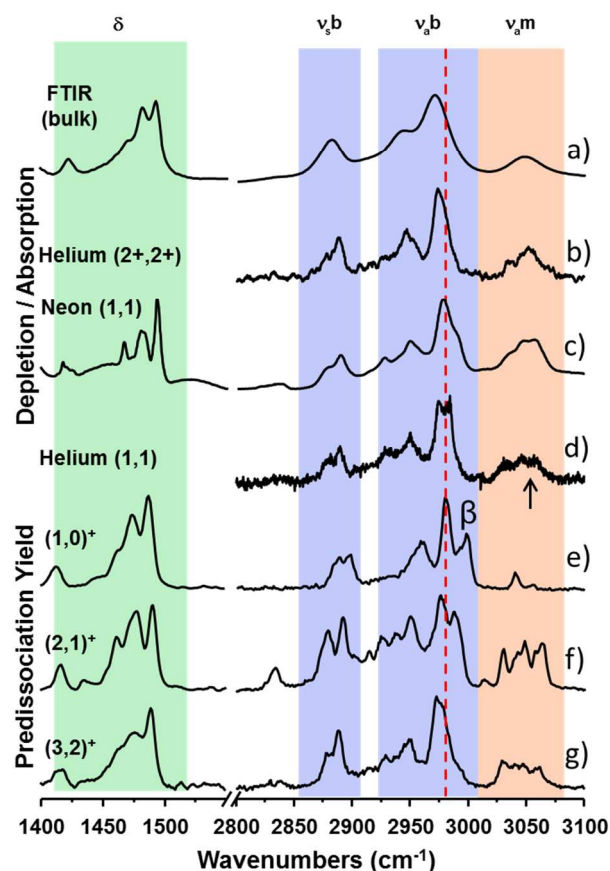


Figure 8. a) FT-IR bulk spectrum of $[\text{NC}_{4111}][\text{NTf}_2]$, b) IR spectrum of neutral ion pairs including at least 2 ion pairs detected mass selective on $m/z = 512$ in helium droplets at an oven temperature of 510(1)K (Helium (2+,2+)), c) IR spectrum of the ion pair $[\text{NC}_{4111}][\text{NTf}_2]$ in a neon matrix (Neon (1,1)), d) (1,1) Ion pair monitored in helium droplets at $m/z \geq 8$, the oven temperature was set to 450(1)K, where 1:1 clusters dominate the spectrum (Helium (1,1)), e-f) CIVP spectra of the (1,0), (2,1) and (3,2) clusters, respectively. The peak labelled β is assigned to the butyl group of the bare cation. The arrow in e) marks the position of the VTMA measurement in the next section. Note that the vertical axes are arbitrarily scaled.

is extracted and is therefore labeled Helium (2+,2+) to emphasize that three or more pairs may contribute to the observed spectrum. In order to be able to form higher clusters, the oven temperature had to be increased from 450 K to 510 K, which increases the vapor pressure and thus the probability of the pick up of more than one $[\text{NC}_{4111}][\text{NTf}_2]$ ion pair. Interestingly, the (2+,2+) neutral ion pairs in helium droplets yield a CH stretching pattern in closest agreement with the bulk FT-IR. The pattern is already evolved from that displayed by the helium (1,1) spectrum with a closer spacing of the strongest asymmetric CH stretches of the butyl chain, suggesting that while electrostatic Coulomb interactions dominate the binding mechanisms in these type of ILs, a further contribution must be attributed to higher order electrostatic interactions, e.g. by dipole dipole, quadrupole–dipole or quadrupole-quadrupole interaction or conformational reorganization upon addition of further charged species.

To further explore the role of pairwise interaction, we invoked measurements of the neutral ion pair in neon and argon matrices. In solid neon, the strongest butyl stretch exhibits a similar peak shape as in helium (1,1), whereas the red-shift found in the bulk is not observed. Measurements in neon and in argon matrices yielded very similar spectra, excluding specific matrix site effects as the cause for the appearance of additional bands.

IVC.1 VTMA in helium nanoparticles

To further explore the assembly motifs in play in the neutral ion pairs, we carried out a series of Stark field experiments which yield additional information on the magnitude of the dipole moment and the relative

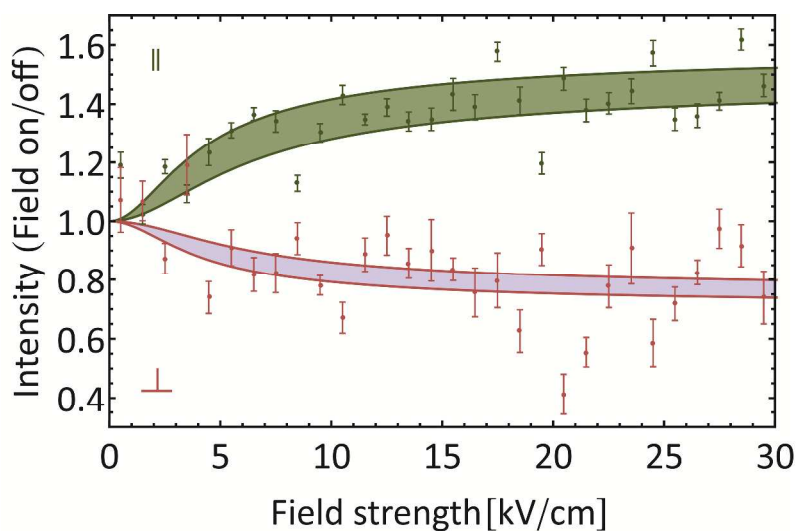


Figure 9. Recorded intensity ratio with field on/off as a function of the electric field strength for the $3054\text{ cm}^{-1}\nu_{\text{am}}$ band marked with arrows in Fig. 6 and 7. Results for the laser polarization parallel/perpendicular to the electric field are displayed in green and red, respectively.

orientation of the dipole moment and the vibrational dipole moment in the isomers of the (1,1) ion pair and the (2,2) pair.

For these measurements we focused on the ν_{am} band at 3054 cm^{-1} , marked with an arrow in Fig. 8, which is expected to have the least overlap with other bands. The field dependence of the peak intensity is recorded using a laser polarization which is parallel and perpendicular to the direction of the applied electric field. This method was first used by Miller and coworkers.^{47,74,75} The field dependence can be used to fit the following two parameters; The permanent dipole moment μ_p and the relative orientation of the vibrational transitional dipole moment $\partial\mu/\partial x_j$, where $\partial\mu/\partial x_j$ describes the derivative of the dipole moment in respect to the respective normal coordinate. Based upon our predictions we expect for the transoid ion pair conformer shown in Fig. 7, a band at 3054 cm^{-1} with a VTMA of 18° and a permanent dipole moment μ_p of 14.8 D. For the *cis* ion pair conformer we predict a band at 3059 cm^{-1} with a VTMA and dipole moment of 43° and 13.8 D, respectively. Fig. 9 shows the recorded intensity dependence on the applied electric field. The laser polarization was chosen to be either parallel with respect to the electric field (green points) or perpendicular (red points). The error bars correspond to one standard deviations after averaging several measurements. We fit the experimental data to two parameters the VTMA α and the permanent dipole moment μ_p , following the paper of Choi *et al.*⁴⁵. As a result, we obtain $\alpha = 44(1)^\circ$ and $\mu_p = 12(3) \text{ D}$. Using these results ($(\alpha \pm \Delta\alpha)$ and $(\mu_p, \pm \Delta\mu_p)$) as input parameters we predict a field dependence within the shaded area in Fig. 9. For the deuterated ion pair ($\text{d}_9\text{-NC}_{4111}$)(NTf₂) we obtain $\alpha = 46(1)^\circ$ and $\mu_p = 10(2) \text{ D}$ at the same IR transitions which are in very good agreement.

The experimental data are in agreement with the predictions for the *cis* ion pair: $\alpha = 43^\circ$ and $\mu_p = 13.8 \text{ D}$. This is surprising in view of the fact that under the conditions of rapid cooling (which should apply in helium clusters) for the supercooled crystallized IL a dominance of (NTf₂)⁻ in transoid configuration has been reported before.³² However, one has to keep in mind that for the predicted energy barrier between the distinct conformers in the (1,1) cluster is very small and several conformers as well as the overlap and mixing of bands might be a problem for an accurate prediction of α . The observed large dipole moment of more than 10 D agrees well with the formation of single polar (1,1) ion pairs in the helium droplet in line with the results for [EMIM][NTf₂].³⁷

Additional measurements at 2890 cm^{-1} and 2950 cm^{-1} in the undeuterated ion pair and at 3029 cm^{-1} and 3045 cm^{-1} in the deuterated cation yielded no field dependence within the experimental uncertainty.

Furthermore, we recorded the electric field dependence upon increasing the temperature in the oven from 490 K to 515 K, thereby increasing the vapor pressure and hence the relative formation of the (2,2) cluster versus the (1,1) cluster. As a result, we obtain at the same frequency (3054 cm^{-1}) a dipole moment of $4(1)\text{ D}$ (see Fig. S3 in the SI). This field dependence resembles a mixture of (1,1), (2,2) and higher clusters which implies that in the (2,2) cluster the dipole moments of the two ion pairs are preferentially aligned almost antiparallel.

At first glance this might be surprising, since the aggregation of building blocks with a large dipole moment (3 D for HCN) has resulted in the formation of chain like structures for HCN aggregates.⁷⁶ This can be explained as a result of long-range dipole-dipole forces acting between two polar molecules which result in the self-assembly of noncovalently bonded linear chains. Dipole-dipole interactions will favor the formation of a cluster with a total dipole moment of $2\mu_p$ (by aligning the dipole moments) yielding the energetically most favorable structure at long range. This long range electrostatic steering at low temperatures has served to explain cluster formation in many cases freezing out even local rather than global minimum structures.⁷⁷

Based upon these results one might expect the formation of an ion pair cluster, where the large dipole moments of each ion pair are aligned. However, we have to take into account that even at temperatures of 0.37 K , several rotational levels will be populated due to the small rotational constants of the ion pairs (all rotational constants are less than 0.01 cm^{-1}). This implies that the dipole-dipole interaction will be motionally averaged scaling as $1/R^6$, with R being the distance between the dipoles (integrated over all angles) instead of scaling as $1/R^3$, thereby greatly reducing its range. As a result, dipole-dipole interactions will play a less important role for the (2,2) ion pair aggregation compared to the case of small polar molecules, where dipole-dipole interaction dominates at long distances and at ultracold temperatures in helium droplets. This also holds for the CIVP measurements of anion-cation clusters where the cluster formation takes place at higher temperatures with a subsequent cooling of the aggregate.

Hence, for higher clusters we expect a less directional van der Waals type like interaction to be structure determining. The averaged electrostatic interaction will lead to a structure with the two dipoles being antiparallel aligned which also corresponds to a local minimum for the dipole-dipole interaction and thus probably to the favored structural motif for the (2,2) building block. The same (rotational averaging) holds in any liquids and might explain why the FTIR IR spectrum of the room temperature ionic liquid agrees very well with the spectrum of the (2,2) cluster.

IVD. The charged clusters

IVD.1 Survey of the trends in the context of inter-molecular interactions between the ions

We next turn to the structural implications of the CIVP spectra of the charged tertiary clusters, which we consider in the context of adding either a cation or anion to the neutral ion pair discussed above.

The relevant spectra are presented in the lower traces of the series presented in Figs. 10 (anions) and 11 (cations). For both charge states, the major trends in the anion-based bands is a red-shifting in the asymmetric SO_2 stretches new 1400 cm^{-1} and the emergence of the α feature near 1150 cm^{-1} in both the (1,2) and (2,1) ions. Interestingly, the transitions throughout the fingerprint region of the (1,2) cluster occur as a series of doublets, most of which were not observed in any of the other complexes investigated here. Those doublets are similar to those present in the CH stretching regions of the (2,1) cation (Fig. 8, second trace from the bottom), hinting that this doubling has a common origin. An obvious

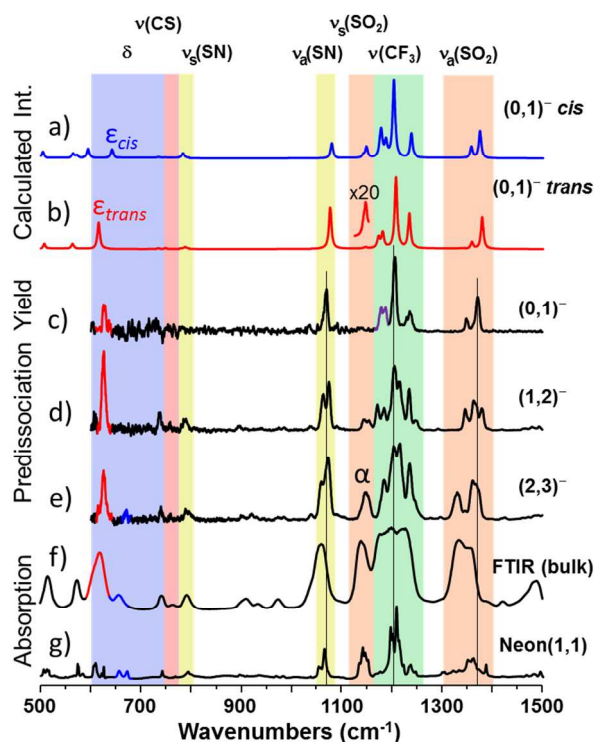


Figure 10. Calculated harmonic spectra for cis (a) and trans (b) conformers of NTf_2^- , c)–e) experimental CIVP spectra of the mass-selected anions with compositions $(\text{NC}_{4111})_n^+ (\text{NTf}_2^-)_{n+1}$, (0,1), (1,2), and (2,3), respectively, f) FTIR of room temperature liquid and g) FTIR spectrum of 1:1 binary complex in a neon matrix.

rationalization for this behavior is to infer that, in the (1,2) case for example, the two $(NTf_2)^-$ anions are bound to the cation at two different sites. It is plausible that one anion adopts the preferred configuration established in the formation of the ion pair, forcing the second anion to attach at a less favorable site. A weaker pairwise interaction would thus yield a small red shift of the key SO_2 stretching bands and thus appear as doubled features in that spectral region. A comparison with the neutral ion pairs in the neon matrix supports the situation in that one peak of the (1,2) doublets has a corresponding matrix feature [e.g., $\nu_a(SO_2)$ near 1348 cm^{-1} and $\nu_a(SN)$ near 1025 cm^{-1}] while the other does not. Note that addition of the second pair manifests itself in a red-shift of the lower energy, in-phase SO_2 stretching modes, asymptotically approaching the bulk limit.

Bands shifts of features associated with the various functional groups also signal the nature of the local interactions between the counter ions. For example, the red-shift of the asymmetric SN stretch ($\nu_a(SN)$) indicates that the cation preferentially binds to the SO_2 groups. Here, a surplus of cations, as is the case in the overall cationic clusters, shifts the SN stretch red by 9 cm^{-1} relative to its bulk value of 1055 cm^{-1} . A lack of $(NC_{4111})^+$ counterparts in the anionic cluster results in a splitting of this band to one transition at the same position as in the bare anion and the other red-shifted towards the bulk limit.

Bands associated with the stretches of the CF_3 group at around 1200 cm^{-1} are not strongly affected by cluster growth. The spectrum of the liquid phase appears featureless in this region with a breadth of nearly 100 cm^{-1} . Nevertheless, the extensive band splitting observed in the (1,2) cluster supports a picture where the deficiency of positive charge carriers forces the second anion to engage in an energetically unfavorable binding geometry, involving the terminal CF_3 groups. In the opposite case, where the anion is sandwiched in between two cations, e.g. the (2,1), the spectrum reproduces the bulk FT-IR spectrum remarkably well, again supporting the role of the excess charge carrier adopting a rather remote, passive position within the cluster, minimally perturbing the core (1,1) ion pair. This differential binding situation is also consistent with the telltale CH stretching modes on the cation, which contribute the pronounced β feature at 2878 cm^{-1} in the bare ion that is conspicuously missing already in the spectrum of the (1,1) complex. The β feature returns in the (2,1) spectrum (Fig. 6) as would be expected if this feature red-shifts and merges with the lower energy bands when the ion locks into the preferred binding site,

leaving the second, more remote cation evidenced by the persistence of the β band. The sensitivity of the butyl CH stretching band to aggregation points to its important role in the overall cluster arrangement, as noted earlier in the context of the co-crystallized domains following slow cooling.³² One could imagine, for example, a case in which the terminal C⁷ methyls of both ion pairs are tethered to the SO₂ and the nitrogen of the excess anion.

IVD.2 Remarks concerning the cis-trans conformations of the anions

An important issue raised earlier is whether the *trans* configuration of the anion, which is most stable in the isolated ion, remains the dominant constituent in the bulk. A telltale feature in this regard is the 625 cm⁻¹ band, ϵ_{trans} , which is unique to the *trans* isomer and is largely due to the shuttle of the N atom between the SO₂ groups. This feature is essentially unshifted, but is significantly enhanced upon addition of ion pairs to form the anionic (1,2) and (2,3) clusters. As such, we conclude that the *trans* form of the anion continues to be the dominant conformer in the negatively charged species. For the larger cluster, however, a small feature is evident around 670 cm⁻¹ close to the calculated feature (ϵ_{cis}) for the *cis* conformer, which is also present as a high energy shoulder in the matrix spectrum of the (1,1) complex. These bands could be identified as a higher energy *cisoid* conformer by subsequently heating IL which was initially frozen out on a CsI window at 4 K up to 300K. In particular, a shoulder at 621 cm⁻¹ (next to the *transoid* anion band at 624 cm⁻¹) and the additional band at 670 cm⁻¹ (next to the *cisoid* anion band at 656 cm⁻¹) gained in intensity after thermal cycling and were thus assigned to higher energy conformers of the *trans* and *cis* configurations, respectively. The behavior of the cationic clusters (2,1) and (3,2) is displayed in Fig. 10. In agreement with the assumption that higher energy conformers are populated in the charged species the ϵ_{trans} band undergoes a stepwise red-shift towards the bulk limit of 617 cm⁻¹ upon addition of the second ion pair while a new band appears close to that expected for ϵ_{cis} .

Herstedt et al. used the relative intensities of the ϵ_{trans} and ϵ_{cis} features as a measure for the relative population of the two conformers.⁷² Following that approach, the ratio of the integrated intensities weighted by the predicted harmonic transition dipole moment for the (2,3) cluster give a value of $R_{exp} = I_{669} / I_{625} = 0.09$. In order to estimate the average number c of anions in *cis* conformation, we use $R_{exp} = (c \cdot I_{cis}) / [(3-c) \cdot I_{trans}]$, for a cluster containing a total

of three anions, yielding $c=0.6$. This analysis indicates that some clusters contain all *trans* anions while others have least one *cis* and two *trans* conformers. On the average 0.6 out of 3 anions (20% of all anions) will be in the *cis* conformation.

In the neon matrix spectrum, two doublets centered at 623 cm^{-1} (621 cm^{-1} and 624 cm^{-1}) and 664 cm^{-1} (656 cm^{-1} and 672 cm^{-1}) could be assigned to the *trans* and conformers, respectively. Thus we conclude that both are present already in the binary complex. Additional temperature dependent measurements confirmed that for each doublet, one peak corresponds to a higher energy conformer trapped in the matrix due to the rapid cooling process. Thus, for the (1,1) cluster in the neon matrix we find a significant population of the *cis* anion, analogous to the situation in the frozen IL.

The effect of pairwise interaction might explain the occurrence of the *cis* conformer in the (2,3) and (3,2) and its absence in the smaller (1,2) and (2,1) complexes: the larger ionic clusters already contain two interacting ion pairs in an antiparallel configuration, dominated by higher order electrostatic or van der Waals interactions while the smaller aggregates are dominated by dipole-charge interaction. The latter ones do not show the presence of the *cis* isomer (resembling more the anion itself). This has to be compared to previous results where anion interaction with the polar part of the cations resulted in polar domains with a preferred population of the *trans* anion conformer while less directional van der Waals interaction between the carbon side chains yielded nonpolar domains with more *cis* anion contribution.³²

The FT-IR spectrum reflects a thermal average of neutral ion pairs in more than one geometric configuration and thus has as well contributions from the *cis* as well as from the *trans*

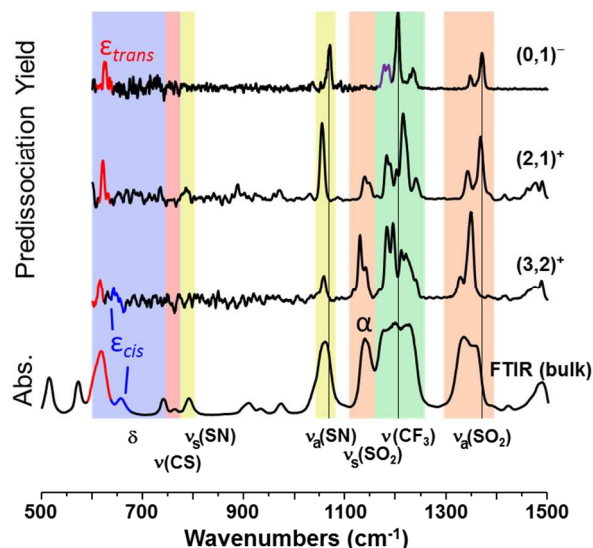


Figure 11. From top to bottom: CIVP spectra of the bare anion (0,1), (2,1) and (3,2) cations, and room temperature FTIR spectrum of the bulk IL. ϵ_{trans} and ϵ_{cis} denote key features used to quantify the contributions of the *cis* and *trans* conformers of the NTf_2 anion in the cluster ensembles.

conformer as does the (1,1) spectrum in neon matrix. In the previous Raman measurements, it was stated that the population of the *cis* conformer goes along with a higher flexibility of the butyl binding conformations. It is thus not surprising that also in the cation frequency range the (1,1) spectrum in neon resembles already that of the bulk at room temperature. Isomers of the neutral ion pair include both structural changes of the individual cations and anions followed by a change of the local docking geometry.

V. Summary

This study explores the molecular level motions underlying the IR spectra of the ionic liquid $[\text{NC}_{4111}][\text{NTf}_2]$ and its deuterated isotopomer $[\text{d}_9\text{-NC}_{4111}][\text{NTf}_2]$ by first isolating the spectra of charged ionic building blocks using mass-selective CIVP spectroscopy and then following the evolution of these bands upon formation of the neutral ion pairs using superfluid helium droplets as well as a solid neon matrix. Site-specific deuteration of the entire butyl chain yielded spectroscopic isolation of the associated stretches from the motions originating from the methyl groups, a key advantage to identify the primary involvement of the latter, when the cation is complexed with the counter anion to form larger neutral and charged clusters.

Larger charged aggregates were then studied again with CIVP. The intrinsic spectra of the isolated ionic constituents, which had previously only been calculated, were obtained with CIVP and compared to *ab initio* electronic structure calculations to identify two different conformers and establish unambiguous assignments for key features arising from each isolated charge carrier. Upon formation of larger clusters with compositions $(\text{NC}_{4111})^+_n(\text{NTf}_2)^-_m$, with $n,m = 0-3$, we observe minor band shifts indicating weak and likely non-directional electrostatic interactions, consistent with a minimal role for hydrogen bonding. The effects of limited ionic constituents, inevitable in charged clusters, led to the population of a remote unfavorable position on the (1,1) core. In general, the cluster spectra are similar to that of the bulk, with the (2+,2+) system displaying the closest resemblance. In the (2,2) arrangement, the ions adopt an antiparallel configuration with less directional interaction. The role of an extra anion or cation attached to both, the (1,1) and the (2,2) ion pairs, is discussed in the context of an additional remote binding site intrinsic to the nature of the ionic IL clusters and as such not anticipated in the bulk phase.

Acknowledgement

We thank Lena Grimmelsmann and Raffael Schwan for their help during the measurements and Teemu Salmi for starting the theoretical predictions. This work was financially supported by the Cluster of Excellence RESOLV (EXC 1069) funded by the Deutsche Forschungsgemeinschaft DFG. MAJ thanks the Department of Energy under grant DE-FG02-06ER15800 for support of this work. E.S-G thanks the Fonds der Chemischen Industrie for a Liebig Stipend.

References

- (1) Ludwig, R.; Kragl, U., Do We Understand the Volatility of Ionic Liquids?, *Angew. Chem. Int. Ed.*, **2007**, *46*, 6582-6584.
- (2) Yu, G. R.; Zhao, D. C.; Wen, L.; Yang, S. D.; Chen, X. C., Viscosity of Ionic Liquids: Database, Observation, and Quantitative Structure-Property Relationship Analysis, *Aiche Journal*, **2012**, *58*, 2885-2899.
- (3) Paulechka, Y. U.; Kabo, A. G.; Blokhin, A. V.; Kabo, G. J.; Shevelyova, M. P., Heat Capacity of Ionic Liquids: Experimental Determination and Correlations with Molar Volume, *Journal of Chemical and Engineering Data*, **2010**, *55*, 2719-2724.
- (4) US Secretary of Commerce, I. L. D. I. T. 2014.
- (5) Hallett, J. P.; Welton, T., Room-Temperature Ionic Liquids: Solvents for Synthesis and Catalysis. 2, *Chem. Rev.*, **2011**, *111*, 3508-3576.
- (6) Freudenmann, D.; Wolf, S.; Wolff, M.; Feldmann, C., Ionic Liquids: New Perspectives for Inorganic Synthesis?, *Angew. Chem. Int. Ed.*, **2011**, *50*, 11050-11060.
- (7) Martins, M. A. P.; Frizzo, C. P.; Moreira, D. N.; Zanatta, N.; Bonaccorso, H. G., Ionic Liquids in Heterocyclic Synthesis, *Chem. Rev.*, **2008**, *108*, 2015-2050.
- (8) Wasserscheid, P.; Welton, T. *Ionic Liquids in Synthesis*; 1st ed.; Wiley-VCH: Weinheim, 2003.
- (9) Dupont, J.; de Souza, R. F.; Suarez, P. A. Z., Ionic Liquid (Molten Salt) Phase Organometallic Catalysis, *Chem. Rev.*, **2002**, *102*, 3667-3691.
- (10) van Rantwijk, F.; Sheldon, R. A., Biocatalysis in Ionic Liquids, *Chem. Rev.*, **2007**, *107*, 2757-2785.
- (11) Song, C. E., Enantioselective Chemo- and Bio-Catalysis in Ionic Liquids, *Chemical Communications*, **2004**, 1033-1043.
- (12) Weingartner, H.; Cabrele, C.; Herrmann, C., How Ionic Liquids Can Help to Stabilize Native Proteins, *Physical Chemistry Chemical Physics*, **2012**, *14*, 415-426.
- (13) Hapiot, P.; Lagrost, C., Electrochemical Reactivity in Room-Temperature Ionic Liquids, *Chem. Rev.*, **2008**, *108*, 2238-2264.
- (14) Lei, Z. G.; Dai, C. N.; Chen, B. H., Gas Solubility in Ionic Liquids, *Chem. Rev.*, **2014**, *114*, 1289-1326.
- (15) Rosen, B. A.; Salehi-Khojin, A.; Thorson, M. R.; Zhu, W.; Whipple, D. T.; Kenis, P. J. A.; Masel, R. I., Ionic Liquid-Mediated Selective Conversion of CO₂ to CO at Low Overpotentials, *Science*, **2011**, *334*, 643-644.

- (16) Scrosati, B.; Hassoun, J.; Sun, Y. K., Lithium-Ion Batteries. A Look into the Future, *Energy & Environmental Science*, **2011**, *4*, 3287-3295.
- (17) Galinski, M.; Lewandowski, A.; Stepniak, I., Ionic Liquids as Electrolytes, *Electrochimica Acta*, **2006**, *51*, 5567-5580.
- (18) Armand, M.; Endres, F.; MacFarlane, D. R.; Ohno, H.; Scrosati, B., Ionic-Liquid Materials for the Electrochemical Challenges of the Future, *Nature Materials*, **2009**, *8*, 621-629.
- (19) Devanathan, R., Recent Developments in Proton Exchange Membranes for Fuel Cells, *Energ. Environ. Sci.*, **2008**, *1*, 101-119.
- (20) Noda, A.; Susan, A. B.; Kudo, K.; Mitsushima, S.; Hayamizu, K.; Watanabe, M., Bronsted Acid-Base Ionic Liquids as Proton-Conducting Nonaqueous Electrolytes, *J. Phys. Chem. B*, **2003**, *107*, 4024-4033.
- (21) de Souza, R. F.; Padilha, J. C.; Goncalves, R. S.; Dupont, J., Room Temperature Dialkylimidazolium Ionic Liquid-Based Fuel Cells, *Electrochemistry Communications*, **2003**, *5*, 728-731.
- (22) Wishart, J. F., Energy Applications of Ionic Liquids, *Energy & Environmental Science*, **2009**, *2*, 956-961.
- (23) Zhang, Y. Q.; Gao, H. X.; Joo, Y. H.; Shreeve, J. M., Ionic Liquids as Hypergolic Fuels, *Angew. Chem. Int. Ed.*, **2011**, *50*, 9554-9562.
- (24) Earle, M. J.; Esperanca, J. M. S. S.; Gilea, M. A.; Lopes, J. N. C.; Rebelo, L. P. N.; Magee, J. W.; Seddon, K. R.; Widgren, J. A., The Distillation and Volatility of Ionic Liquids, *Nature*, **2006**, *439*, 831-834.
- (25) Neto, B. A. D.; Santos, L. S.; Nachtigall, F. M.; Eberlin, M. N.; Dupont, J., On the Species Involved in the Vaporization of Imidazolium Ionic Liquids in a Steam-Distillation-Like Process, *Angewandte Chemie-International Edition*, **2006**, *45*, 7251-7254.
- (26) Chen, H.; Zheng, O. Y.; Cooks, R. G., Thermal Production and Reactions of Organic Ions at Atmospheric Pressure, *Angewandte Chemie-International Edition*, **2006**, *45*, 3656-3660.
- (27) Dong, K.; Zhao, L. D.; Wang, Q.; Song, Y. T.; Zhang, S. J., Are Ionic Liquids Pairwise in Gas Phase? A Cluster Approach and in Situ IR Study, *Phys. Chem. Chem. Phys.*, **2013**, *15*, 6034-6040.
- (28) Leal, J. P.; Esperanca, J. M. S. S.; da Piedade, M. E. M.; Lopes, J. N. C.; Rebelo, L. P. N.; Seddon, K. R., The Nature of Ionic Liquids in the Gas Phase, *Journal of Physical Chemistry A*, **2007**, *111*, 6176-6182.
- (29) Heimer, N. E.; Del Sesto, R. E.; Meng, Z. Z.; Wilkes, J. S.; Carper, W. R., Vibrational Spectra of Imidazolium Tetrafluoroborate Ionic Liquids, *J. Mol. Liq.*, **2006**, *124*, 84-95.
- (30) Fumino, K.; Wulf, A.; Ludwig, R., Strong, Localized, and Directional Hydrogen Bonds Fluidize Ionic Liquids, *Angew. Chem. Int. Ed.*, **2008**, *47*, 8731-8734.
- (31) Katsyuba, S. A.; Zvereva, E. E.; Vidis, A.; Dyson, P. J., Application of Density Functional Theory and Vibrational Spectroscopy toward the Rational Design of Ionic Liquids, *J. Phys. Chem. A*, **2007**, *111*, 352-370.
- (32) Faria, L. F. O.; Matos, J. R.; Ribeiro, M. C. C., Thermal Analysis and Raman Spectra of Different Phases of the Ionic Liquid Butyltrimethylammonium Bis(Trifluoromethylsulfonyl)Imide, *J. Phys. Chem. B*, **2012**, *116*, 9238-9245.
- (33) Desiraju, G. R., The C-H Center Dot Center Dot Center Dot O Hydrogen Bond: Structural Implications and Supramolecular Design, *Accounts of Chemical Research*, **1996**, *29*, 441-449.
- (34) Bini, R.; Bortolini, O.; Chiappe, C.; Pieraccini, D.; Siciliano, T., Development of Cation/Anion "Interaction" Scales for Ionic Liquids through Esi-MS Measurements, *J. Phys. Chem. B*, **2007**, *111*, 598-604.

- (35) Niedermeyer, H.; Ashworth, C.; Brandt, A.; Welton, T.; Hunt, P. A., A Step Towards the a Priori Design of Ionic Liquids, *Physical Chemistry Chemical Physics*, **2013**, *15*, 11566-11578.
- (36) Cooper, R.; Zolot, A. M.; Boatz, J. A.; Sporleder, D. P.; Stearns, J. A., Ir and Uv Spectroscopy of Vapor-Phase Jet-Cooled Ionic Liquid $\text{Emim}^+ \text{Tf}_2\text{n}^-$: Ion Pair Structure and Photodissociation Dynamics, *J. Phys. Chem. A*, **2013**, *117*, 12419-12428.
- (37) Obi, E. I.; Leavitt, C. M.; Raston, P. L.; Moradi, C. P.; Flynn, S. D.; Vaghjiani, G. L.; Boatz, J. A.; Chambreau, S. D.; Douberly, G. E., Helium Nanodroplet Isolation and Infrared Spectroscopy of the Isolated Ion-Pair 1-Ethyl-3-Methylimidazolium Bis(Trifluoromethylsulfonyl)Imide, *J. Phys. Chem. A*, **2013**, *117*, 9047-9056.
- (38) Johnson, C. J.; Fournier, J. A.; Wolke, C. T.; Johnson, M. A., Ionic Liquids from the Bottom Up: Local Assembly Motifs in $[\text{Emim}][\text{Bf}_4]$ through Cryogenic Ion Spectroscopy, *Journal of Chemical Physics*, **2013**, *139*, 224305.
- (39) Fournier, J. A.; Wolke, C. T.; Johnson, C. J.; McCoy, A. B.; Johnson, M. A., Comparison of the Local Binding Motifs in the Imidazolium-Based Ionic Liquids $[\text{Emim}][\text{Bf}_4]$ and $[\text{Emmim}][\text{Bf}_4]$ through Cryogenic Ion Vibrational Predissociation Spectroscopy: Unraveling the Roles of Anharmonicity and Intermolecular Interactions, *Journal of Chemical Physics*, **2014**, *submitted*.
- (40) Dhumal, N. R.; Noack, K.; Kiefer, J.; Kim, H. J., Molecular Structure and Interactions in the Ionic Liquid 1-Ethyl-3-Methylimidazolium Bis(Trifluoromethylsulfonyl)Imide, *J. Phys. Chem. A*, **2014**, *118*, 2547-2557.
- (41) Vyas, S.; Dreyer, C.; Slingsby, J.; Bicknese, D.; Porter, J. M.; Maupin, C. M., Electronic Structure and Spectroscopic Analysis of 1-Ethyl-3-Methylimidazolium Bis(Trifluoromethylsulfonyl)Imide Ion Pair, *J. Phys. Chem. A*, **2014**, *118*, 6873-6882.
- (42) Kamrath, M. Z.; Garand, E.; Jordan, P. A.; Leavitt, C. M.; Wolk, A. B.; Van Stipdonk, M. J.; Miller, S. J.; Johnson, M. A., Vibrational Characterization of Simple Peptides Using Cryogenic Infrared Photodissociation of H_2 -Tagged, Mass-Selected Ions, *J. Am. Chem. Soc.*, **2011**, *133*, 6440-6448.
- (43) Wolk, A. B.; Leavitt, C. M.; Garand, E.; Johnson, M. A., Cryogenic Ion Chemistry and Spectroscopy, *Acc. Chem. Res.*, **2014**, *47*, 202-210.
- (44) Goyal, S.; Schutt, D. L.; Scoles, G., Vibrational Spectroscopy of Sulfur-Hexafluoride Attached to Helium Clusters, *Physical Review Letters*, **1992**, *69*, 933-936.
- (45) Scoles, G.; Lehmann, K. K., Molecular Spectroscopy - Nanomatrices Are Cool, *Science*, **2000**, *287*, 2429-2430.
- (46) Toennies, J. P.; Vilesov, A. F., Superfluid Helium Droplets: A Uniquely Cold Nanomatrix for Molecules and Molecular Complexes, *Angew. Chem. Int. Ed.*, **2004**, *43*, 2622-2648.
- (47) Choi, M. Y.; Douberly, G. E.; Falconer, T. M.; Lewis, W. K.; Lindsay, C. M.; Merritt, J. M.; Stiles, P. L.; Miller, R. E., Infrared Spectroscopy of Helium Nanodroplets: Novel Methods for Physics and Chemistry, *Int. Rev. Phys. Chem.*, **2006**, *25*, 15-75.
- (48) Khriachtchev, L., Rotational Isomers of Small Molecules in Noble-Gas Solids: From Monomers to Hydrogen-Bonded Complexes, *Journal of Molecular Structure*, **2008**, *880*, 14-22.
- (49) Hanke, K.; Nieto, P.; Poerschke, T.; Schwaab, G.; Havenith, M. In *22nd High Resolution Molecular Spectroscopy* Dijon, France, 2011.
- (50) von Haeften, K.; Rudolph, S.; Simanovski, I.; Havenith, M.; Zillich, R. E.; Whaley, K. B., Probing Phonon-Rotation Coupling in Helium Nanodroplets: Infrared Spectroscopy of Co and Its Isotopomers, *Physical Review B*, **2006**, *73*.

- (51) Kong, W.; Pei, L. S.; Zhang, J., Linear Dichroism Spectroscopy of Gas Phase Biological Molecules Embedded in Superfluid Helium Droplets, *International Reviews in Physical Chemistry*, **2009**, *28*, 33-52.
- (52) GmbH, U. o. K. a. F. K.; TURBOMOLE GmbH, since 2007: Karlsruhe, Germany, 1989.
- (53) Becke, A. D., Density-Functional Thermochemistry Iii. The Role of Exact Exchange, *Journal of Chemical Physics*, **1993**, *98*, 5648-5652.
- (54) Stephens, P. J.; Devlin, F. J.; Chabalowski, C. F.; Frisch, M. J., Ab Initio Calculation of Vibrational Absorption and Circular Dichroism Spectra Using Density Functional Force Fields, *J. Phys. Chem.*, **1994**, *98*, 11623-11627.
- (55) Kendall, R. A.; Dunning, T. H., Jr.; Harrison, R. J., Electron Affinities of the First-Row Atoms Revisited. Systematic Basis Sets and Wave Functions., *Journal of Chemical Physics*, **1992**, *96*, 6796-6806.
- (56) Woon, D. E.; Dunning, T. H., Jr., Electron Affinities of the First-Row Atoms Revisited. Systematic Basis Sets and Wave Functions, *Journal of Chemical Physics*, **1993**, *98*, 1358.
- (57) Schäfer, A. H., H.; Ahlrichs, R., Fully Optimized Contracted Gaussian Basis Sets for Atoms Li to Kr, *Journal of Chemical Physics*, **1992**, *97*.
- (58) Grimme, S., Semiempirical Gga-Type Density Functional Constructed with a Long-Range Dispersion Correction, *J. Comput. Chem.*, **2006**, *27*, 1787-1799.
- (59) Arnim, M. v. A., R., Parallelization of Density Functional and Ri-Coulomb Approximation in Turbomole *J. Comp. Chem.*, **1998**, *19*.
- (60) Weigend, F.; Häser, M., Ri-Mp2: First Derivatives and Global Consistency *Theo. Chem. Acc.*, **1997**, *97*, 331.
- (61) Deglmann, P. F., F.; Ahlrichs, R., An Efficient Implementation of Second Analytical Derivatives for Density Functional Methods 511., *Chem. Phys. Letters*, **2002**, *362*.
- (62) Deglmann, P. F., F.; Ahlrichs, R., Efficient Characterization of Stationary Points on Potential Energy Surfaces, *Journal of Chemical Physics*, **2002**, *117*.
- (63) Deglmann, P. M., K.; Furche, F.; Ahlrichs, R., Nuclear Second Analytical Derivative Calculations Using Auxiliary Basis Set Expansion, *Chem. Phys. Letters*, **2004**, *384*.
- (64) Peterson, K. A. D., Jr., T.H., Accurate Correlation Consistent Basis Sets for Molecular Core-Valence Correlation Effects. The Second Row Atoms Al - Ar, and the First Row Atoms B - Ne Revisited, *Journal of Chemical Physics*, **2002**, *117*.
- (65) Dunning, T. H., Jr., Gaussian Basis Sets for Use in Correlated Molecular Calculations. I. The Atoms Boron through Neon and Hydrogen, *Journal of Chemical Physics*, **1989**, *90*, 1007-1023.
- (66) Woon, D. E. D., Jr. T. H., Gaussian Basis Sets for Use in Correlated Molecular Calculations. Iii. The Second Row Atoms, Al-Ar *Journal of Chemical Physics*, **1993**, *98*.
- (67) Sherwood, P. V., A. H. d.; Guest, M. F.; Schreckenbach, G.; Catlow, C. R. A.; French, S. A.; Sokol, A. A.; Bromley, S. T.; Thiel, W.; Turner, A. J.; Billeter, S.; Terstegen, F.; Thiel, S.; Kendrick, J.; Rogers, S. C.; Casci, J.; Watson, M.; King, F.; Karlsen, E.; Sjøvoll, M.; Fahmi, A.; Schäfer, A.; Lennartz, C., Quasi: A General Purpose Implementation of the Qm/Mm Approach and Its Application to Problems in Catalysis, *J. Mol. Struct.-Theochem.*, **2003**, *632*, 1-28.
- (68) Metz, S.; Kastner, J.; Sokol, A. A.; Keal, T. W.; Sherwood, P., Chemshell - a Modular Software Package for Qm/Mm Simulations, *Wiley Interdisciplinary Reviews-Computational Molecular Science*, **2014**, *4*, 101-110.
- (69) Klyne, W.; Prelog, V., Description of Steric Relationships across Single Bonds, *Experientia*, **1960**, *16*, 521-523.

- (70) Fujimori, T.; Fujii, K.; Kanzaki, R.; Chiba, K.; Yamamoto, H.; Umebayashi, Y.; Ishiguro, S. I., Conformational Structure of Room Temperature Ionic Liquid N-Butyl-N-Methyl-Pyrrolidinium Bis(Trifluoromethanesulfonyl) Imide - Raman Spectroscopic Study and Dft Calculations, *Journal of Molecular Liquids*, **2007**, *131*, 216-224.
- (71) Holomb, R.; Martinelli, A.; Albinsson, I.; Lassegues, J. C.; Johansson, P.; Jacobsson, P., Ionic Liquid Structure: The Conformational Isomerism in 1-Butyl-3-Methyl-Imidazolium Tetrafluoroborate (Bmim Bf₄), *J. Raman. Spectrosc.*, **2008**, *39*, 793-805.
- (72) Herstedt, M.; Smirnov, M.; Johansson, P.; Chami, M.; Grondin, J.; Servant, L.; Lassegues, J. C., Spectroscopic Characterization of the Conformational States of the Bis (Trifluoromethanesulfonyl)Imide Anion (Tfsi⁻), *J. Raman Spectrosc.*, **2005**, *36*, 762-770.
- (73) Brouillette, D.; Irish, D. E.; Taylor, N. J.; Perron, G.; Odziemkowski, M.; Desnoyers, J. E., Stable Solvates in Solution of Lithium Bis(Trifluoromethylsulfone)Imide in Glymes and Other Aprotic Solvents: Phase Diagrams, Crystallography and Raman Spectroscopy, *Physical Chemistry Chemical Physics*, **2002**, *4*, 6063-6071.
- (74) Choi, M. Y.; Miller, R. E., Four Tautomers of Isolated Guanine from Infrared Laser Spectroscopy in Helium Nanodroplets, *J. Am. Chem. Soc.*, **2006**, *128*, 7320-7328.
- (75) Dong, F.; Miller, R. E., Vibrational Transition Moment Angles in Isolated Biomolecules: A Structural Tool, *Science*, **2002**, *298*, 1227-1230.
- (76) Nauta, K.; Miller, R. E., Nonequilibrium Self-Assembly of Long Chains of Polar Molecules in Superfluid Helium, *Science*, **1999**, *283*, 1895-1897.
- (77) Madeja, F.; Havenith, M.; Nauta, K.; Miller, R. E.; Chocholousova, J.; Hobza, P., Polar Isomer of Formic Acid Dimers Formed in Helium Nanodroplets, *Journal of Chemical Physics*, **2004**, *120*, 10554-10560.